# Nonlinear dynamics of coupled charged rotators

Shinji Chiba,*,† and Yasuji Sawada‡
*Research Institute of Electrical Communication, Tohoku University, 2-1-1 Katahira, Aoba-ku, Sendai 980-77, Japan*
(Received 10 February 1997)

A needle rotator system is constructed and investigated as a model system for coupled oscillators with nonlocal interaction. Needle rotators placed in a strong homogeneous electrical field rotate by repulsive or attractive force between the electrodes and charge on the rotators created by the discharge. The charge on the rotators is simultaneously the source of long-range interaction between the rotators. This paper describes the case where all rotators were placed an equal distance from each other on a horizontal line perpendicularly to the homogeneous field, and where the sense of the rotation were the same. The experimental results show entrainment, hysteresis, multistability, and chaos phenomena in the coupled dynamics of the rotator system. Simulation of the needle rotator carried out using a model regarding the shape of the rotator as a L-shaped line reproduced the global features of dynamics of the rotator system. The possibility is discussed of whether a system consisting of needle rotators presents a real system of a coupled oscillator system with nonlocal interaction. [S1063-651X(97)03809-9]

PACS number(s): 05.45.+b

## I. INTRODUCTION

Dynamical systems with nonlocal interaction have been studied in various fields of science. A biological neural network is one system of this class. Experimental results showed that a collective behavior of many neurons in a central nervous system affected to recognition [1,2]. Dynamics of some physical systems such as the Josephson junction array and charged density wave may also belong to this class system, and were modeled by coupled oscillators with global interaction [3,4].

Recently, coupled oscillations with nonlocal interaction have been studied theoretically [5,6]. When the interaction is of a middle range in strength, the appearance of microchaos and macrochaos was reported in the globally coupled Ginzburg-Landau system [5]. Numerical experiments showed that a coupled oscillator system with long-range coupling had unique dynamics in the collective behavior of the system. A model system in one-dimensional space showed that the correlations and fluctuations obeyed a power law and that the exponents change continuously with the coupling strength [5]. A small number of clusters, a continuous string-like distribution, and chaotic dynamics appeared in the phase plane as a change of coupling strength [6]. However, no real system has been proposed for which we can perform detailed experimental study of oscillators with long-range coupling.

Previously we reported briefly on experimental results of a pair of rotators for studying coupled oscillators with nonlocal interaction [7]. In this paper we describe in detail the dynamics of coupled needle rotator systems interacting with each other by Coulomb force, including locking, hysteresis, and chaos, together with a numerical simulation.

## II. EXPERIMENTAL SYSTEM

A needle rotator is a rotator which rotates in a strong electric field. The rotator used in the present experiment is the simplest needle rotator one can think of, composed of conductive needles as shown in Fig. 1. Discharge takes place if the field intensity at the edge exceeds a threshold when the arm of the rotator is at a position nearly parallel to the external field. The sign of the discharge depends on whether the arm edge of the rotator is close to the positive or negative electrode. The arm is forced to rotate by the Coulomb interaction between the continuous charge distribution over the horizontal arm and the external field.

The experimental system of the present study is described as follows. Needle rotators were placed, equally distanced, on a horizontal line parallel to two planar electrodes of $200\times 500\ \mathrm{mm}^2$, 53 mm apart from each other. The applied electric field was varied from 3.0 to 4.5 kV/cm. The vertical arms of these rotators were electrically connected through

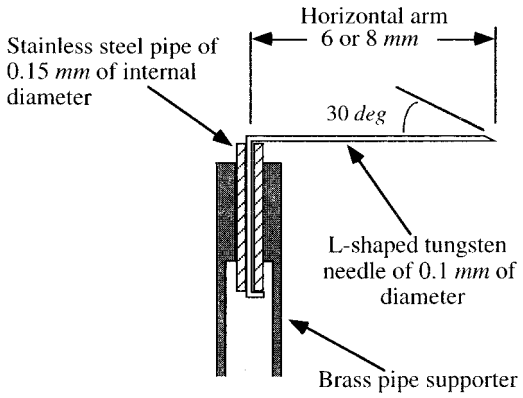


FIG. 1. Schematic view of a needle rotator.

*Present address: Sendai National College of Technology, Kamiayashi, Aoba-ku, Sendai 989-31, Japan.
†Electronic address: chiba@info.sendai-ct.ac.jp
‡Electronic address: sawada@sawada.riec.tohoku.ac.jp

 

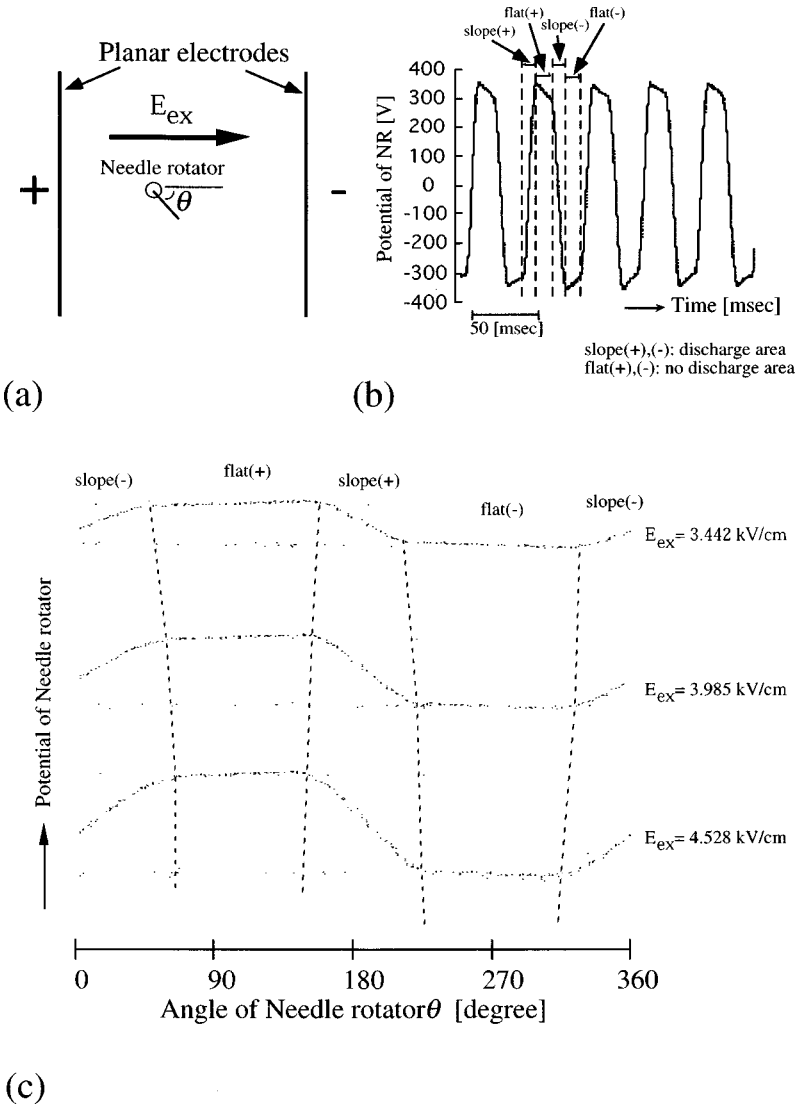


FIG. 2. (a) Configuration of one rotator between two planer electrodes. (b) Typical potential waveform of a single rotator. (c) Characteristics of the angle of the needle rotator vs the potential of a needle rotator. The sampling rate of the angle by the video is 33.3 ms, while the typical period of rotation is 50 ms. Therefore, the plotted angles are the collection of sampled angles measured over several hundred cycles. The plots for the cases for three different external field $E_{ex}$ are shown. The dotted lines are the rough border between different states of discharge.

the outer pipe to a capacitor whose partial voltage was measured by a sampling recorder with sampling time of 100 $\mu$s. Rotating motion of these rotators were recorded by Hi8 video cassette recorder and the angles of these rotators were measured by every 1 flame of the video tape by a computer.

## III. EXPERIMENTAL RESULT

### Single rotator

A typical waveform of the electric potential of one rotating needle rotator [Fig. 2(a)] is illustrated in Fig. 2(b). The waveform consists of two different parts. One is a positive or negative steep slope zone, called slope(+) and slope(−), respectively, and the other is a flat zone called flat(+) or flat(−), respectively. Figure 2(c) shows the dependence of the potential on the angle of the needle. As seen in Fig. 2(c), a zone of slope(+)(−) corresponding to an electrical discharge around $\theta=0°$ or 180°, at which the electrical field on the pointed edge of the horizontal arm was the strongest.

### Stationary state

There are two types of stationary states depending on initial conditions with different angles of the rotator. When $\theta_{init}=120°$, the stationary state is a stable fixed point with $\theta_{\infty}=180°$ with damping vibration [see Fig. 3(a)]. The flat potential seen in Fig. 3(a) means no discharge. On the other hand, for $\theta_{init}=110°$ the stationary state is a periodic motion [see Fig. 3(b)]. The choice of the stationary states was decided depending whether the rotator could go through the torque reversing area near $\theta=0°$ or 180° by the inertia.

$\dot{\theta}$ could not be measured in this experiment because the sampling rate of the $\theta$ is much slower than the period of the rotation. Figure 4 shows the $\theta$-$\dot{\theta}$ plane calculated by a model of the rotator presented in Sec. IV. This figure indicates that there are two stable fixed points and two periodic orbits in the dynamics of the rotator.

### Mean rotation period

The dependence of mean rotation period of rotator on external field and mean peak to peak amplitude of that are shown in Fig. 5(a). With increasing external field the charge of the rotator and thereby its rotation period increase.

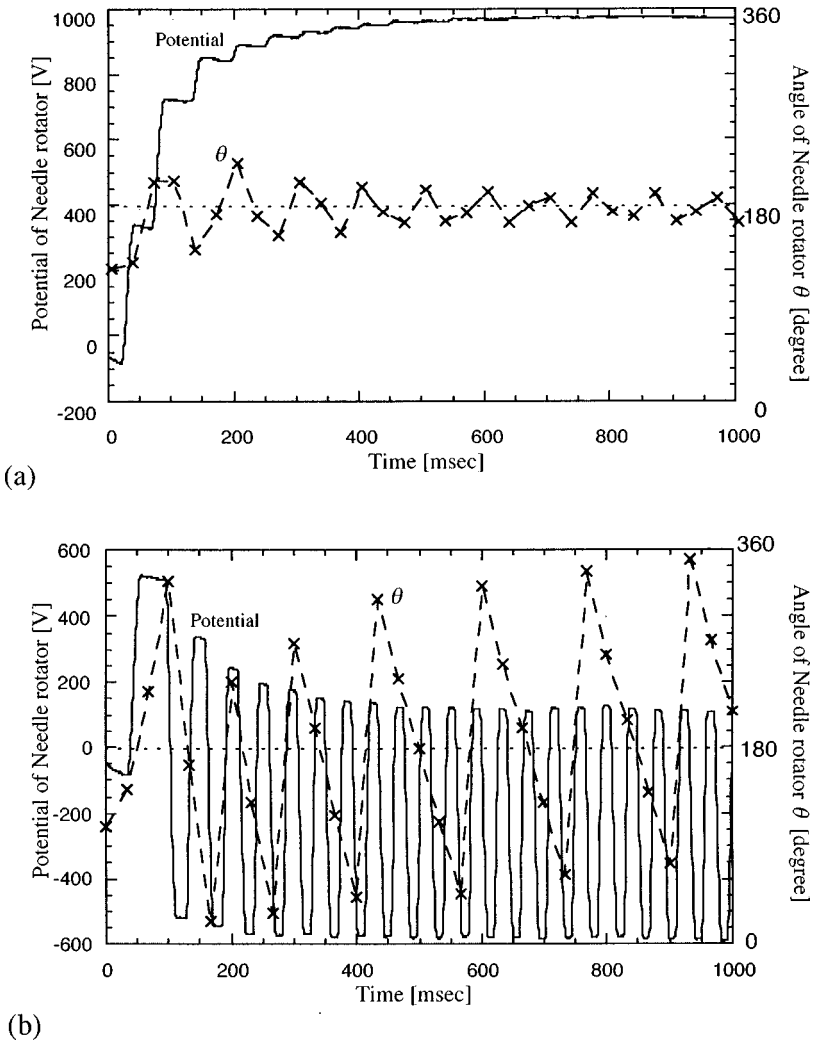


FIG. 3. Two stationary states transited from different initial conditions. The initial conditions were given by the step input of an external field of 4 kV/cm, when the rotator is standing still at an initial angle $\theta_{\text{init}}$ with (a) $\theta_{\text{init}}=120°$ (damping vibration) and (b) $\theta_{\text{init}}=110°$ (nonlinear rotation).

### Two-rotator system

One rotator having an arm length of 8 mm (NR1), and another having one of 6 mm (NR2), were used in this experiment. The configuration in an applied field is illustrated in Fig. 5(b). Some variables for describing the interaction of the two rotators are defined in Fig. 5(c). $t_i(n)$ is the $n$th termination time of the positive discharge of the $i$th needle rotator (NR$i$). $T_i(t_j(n))$ means the time duration of the potential variation of NR$i$ which includes $t_j(n)$. $\psi_i(t_j(n))$ is the phase value of $t_j(n)$ measured with respect to $T_i(t_j(n))$. This value takes a value from 0 to 1, corresponding to the start and end of $T_i(t_j(n))$, respectively. The mutual behavior of the two rotators depends on the difference in the arm lengths, the distance between the two rotators, the senses of the two rotators (the same direction in the present work), and the applied field strength (varied from 3.17 to 4.53 kV/cm in the present work).

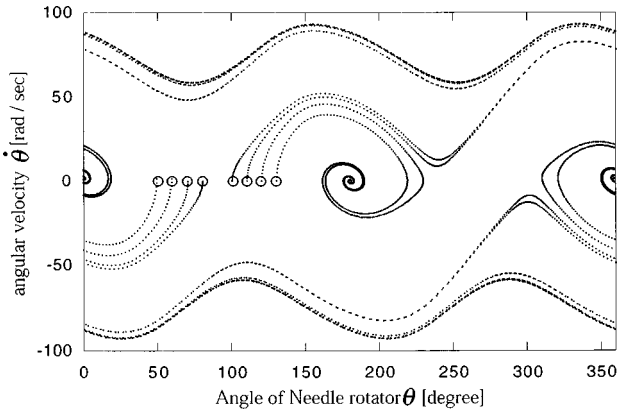


FIG. 4. A behavior of a single rotator in the $\theta$-$\dot{\theta}$ plane. The parameters of the rotator are shown in column NR2 of Table I. This figure shows orbits from some initial points indicated by circles.

### Bifurcation diagram

Figure 6(a) shows an example of the bifurcation diagram of the ratio of the time-averaged period with the applied field as the control parameter, for a fixed distance of 15 mm. When the field was increased from 3.17 kV/cm, 2:1 locked stable states were observed up to 3.44 kV/cm. Then 3:2 locked states (3.53 kV/cm), a 3:2 locked state mixed with an unlocked state (3.62 to 3.71 kV/cm), unlocked states (from 3.80 to 4.26 kV/cm), and a 1:1 coupled state (4.35 to 4.53 kV/cm) were successively observed. When the field was decreased, 1:1 locked states were observed down to 3.99 kV/cm, and then unlocked states (from 3.90 to 3.80 kV/cm),

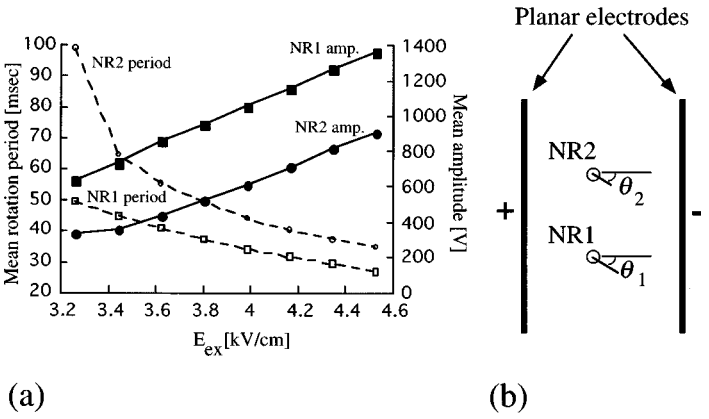


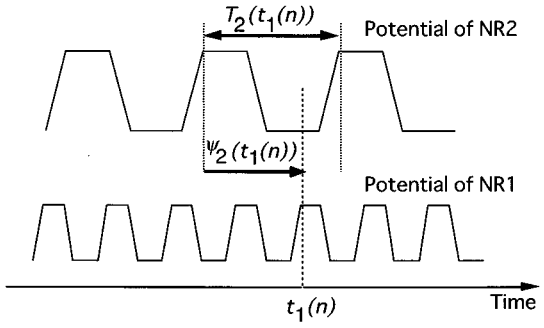


FIG. 5. (a) Characteristics of external field $E_{ex}$ vs the mean rotation period and mean peak-to-peak amplitude of two different rotators with horizontal arm lengths of 6 (NR1) and 8 mm (NR2). (b) Configuration of the two rotators between two planer electrodes. The distance between the two rotators is fixed at 15 mm. (c) Definition of variables from the waveforms of the potential of two rotators. $t_1(n)$ is the termination time of the positive discharge of NR1. $T_2(t_1(n))$ is a time period of NR2 in which $t_1(n)$ is on the time axis. $\psi_2(t_1(n))$ is the phase value of NR2 against NR1. This value changes linearly from 0 to 1 corresponding to the start edge of and end edge of $T_2(t_1(n))$, respectively.

unlocked states mixed with 3:2 locked states (3.71 to 3.62 kV/cm), pure 3:2 states (3.53 to 3.49 kV/cm), and 3:2 states mixed with 2:1 states (3.44 kV/cm) were successively observed. The rotation of NR2 stopped below 3.40 kV/cm, though the field maintained a rotation of NR2 when not interacting with NR1 [Fig. 5(a)]. One can observe hysteresis over the entire region of the applied field, as is often found in a system with coexisting multistable states.

Figure 6(b) and 6(c) show the distribution of the instantaneous relationship between the phase $\psi_2(t_1(n))$ and the ratio of the rotating period $T_2(t_1(n))/T_1(t_1(n))$ for some states in Fig. 6(a). The figures show that there is a continuous permitted range on the axial phase difference for each state. For example, the cluster of the phase difference values $\psi_2(t_1(n))$ for the 1:1 state sifted to zero when the applied field was decreased. This state became unstable at a critical value of the applied field for which the left edge of the cluster for $\psi_2(t_1(n))$ approached 0.2 [see Fig. 6(c)].

### Multirotator system

A basic experiment using six rotators with nominally same arm length was carried out for studying collective behavior of the needle rotator systems. Each rotator had a horizontal arm length of $6 \pm 0.03$ mm and was named NR1,NR2, . . . ,NR6, respectively.

Figure 7(a) shows the mean rotation period of each rotator with the external field. The characteristics were varied $\pm 15\%$ from the mean value, caused by clearance of the connection part between the L-shaped needle and the stainless steel support pipe, and the nonuniformity of the edge shape of the rotator (see Fig. 1).

The relative position of the rotators in the applied field is illustrated in Fig. 7(b). The applied external electrical fields $E_{ex}$ were 3.874, 4.042, and 4.211 kV/cm. The potential values of rotators were measured with a sampling rate of 200 $\mu$s for 2 min. The sense of rotation of all rotators was set same throughout this experiment.

The sequence of phase differences of each rotator with respect to NR4 is shown in Fig. 8. It is seen that all sequence of phase differences are perturbed in a finite range (a typical whole sequence in right column of Fig. 8). This state may be called a synchronous state, since the periods of all rotators were same and the set of phase differences depended on initial conditions. Two synchronous states were seen at $E_{ex}$=4.211 kV/cm. The phase differences of NR1 and NR2 with respect to NR4 were simultaneously from time to time shifted to another stable synchronous state, as shown in Fig. 8.

## IV. NUMERICAL STUDY ON THE DYNAMICS OF THE NEEDLE ROTATOR

The dynamics of the needle rotator system is analyzed numerically in this section. The charge distribution on the horizontal arm and the supporter of the rotator plays a key role for the dynamics of the rotator. The shape of the rotator

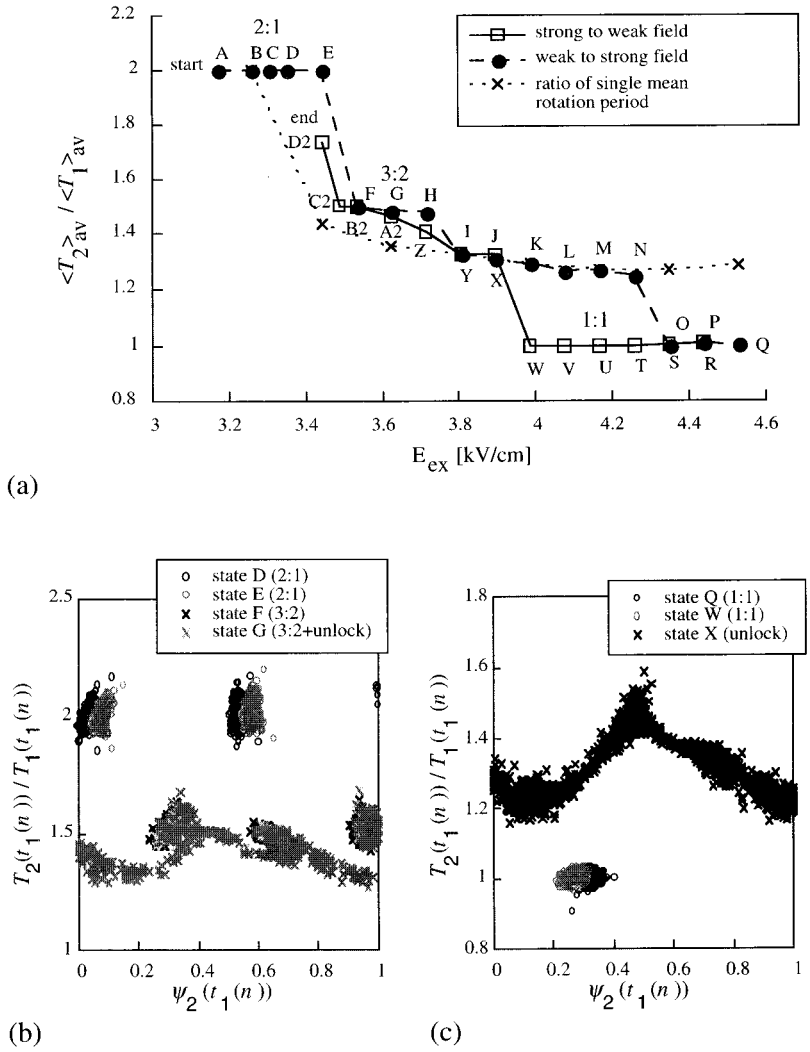


FIG. 6. (a) Example of the bifurcation diagram of a time-averaged period ratio with the applied field $E_{ex}$ as the control parameter. The average was taken for 1-min duration starting after 3-min stabilizing time. The broken and solid lines, respectively, show the time-averaged period ratio when the field is increased and decreased. The dotted line shows the ratio of the time-averaged period of rotators without interaction. (b) The distributions of the instantaneous relationship between the phase $\psi_2(t_1(n))$ and the ratio of rotation periods $T_2(t_1(n))/T_1(t_1(n))$ of four states in the bifurcation diagram when the applied field was increased successively from $D$ to $E$, $F$, and $G$. The ratio of rotation periods was 2:1 at states $D$ and $E$, 3:2 at state $F$, and 3:2 +unlock (irrational ratio) at state $G$. (c) The distributions of three states when the applied field was decreased. The direction of the transition was from state $Q$ to states $W$ and $X$. The ratio of rotation periods was 1:1 at states $Q$ and $W$, and unlock (irrational ratio) at state $X$.

was assumed to be a L-shaped line since the diameter of the rotator was much smaller compared with the length of the needle and the distance between rotators. This means that the charge distribution on the rotator was approximated to a one-dimensional distribution of the L-shaped line. Some values of the L-shaped line are defined as follows. $L$ is the length of horizontal arm of the rotator and $A$ is the length of vertical supporter. This rotator is able to rotate in the $r$-$\theta$ plane and fixed in axial $z$. $\vec{E}_{ex}$ is the homogeneous applied external electric field. The direction of this field is parallel to $r$-$\theta$ plain. $\vec{l}$ and $\vec{m}$ are position vectors on the rotator and $\rho(\vec{l})$ is charge density at $\vec{l}$. When one rotator is placed between the electrodes, the electric field $\vec{E}(\vec{l})$ at $\vec{l}$ on the rotator due to the charge distribution on the rotator is expressed as

$$\vec{E}(\vec{l}) = \frac{1}{4\pi\epsilon} \int_{A+L} \frac{\rho(\vec{m})}{|\vec{m}-\vec{l}|^3}(\vec{m}-\vec{l})dm. \tag{1}$$

The field according to the L-shaped line of a rotator is zero since the rotator is conductor, that is,

$$(\vec{E}(\vec{l})+\vec{E}_{ex})\cdot\vec{z}_0 = \vec{E}(\vec{l})\cdot\vec{z}_0 = 0 \quad (\text{on } A),$$
$$(\vec{E}(\vec{l})+\vec{E}_{ex})\cdot\vec{r}_0 = \vec{E}(\vec{l})\cdot\vec{r}_0 + E_{ex}\cos\theta = 0 \quad (\text{on } L). \tag{2}$$

$\vec{z}_0$ and $\vec{r}_0$ are unit vectors parallel to $z$ axis and to the radial vector $\vec{r}$, respectively. The torque on the horizontal arm of the rotator $\vec{T}$ is

$$\vec{T} = \int_L \rho(\vec{l})\vec{l}\times(\vec{E}(\vec{l})+\vec{E}_{ex})dl. \tag{3}$$

It was assumed in this analysis that the discharge between the rotator and the electrode takes place when the charge density on the edge of the horizontal arm at which $|\vec{l}| = L$ exceeds a threshold $\rho_{th}$, that is

$$\rho(\vec{l}) > \rho_{th}, \quad |\vec{l}| = L. \tag{4}$$

Next, we describe the case where there are $N$ numbers of rotators in the homogeneous electric field. The configuration of the rotators and definition of values are shown in Fig. 9.

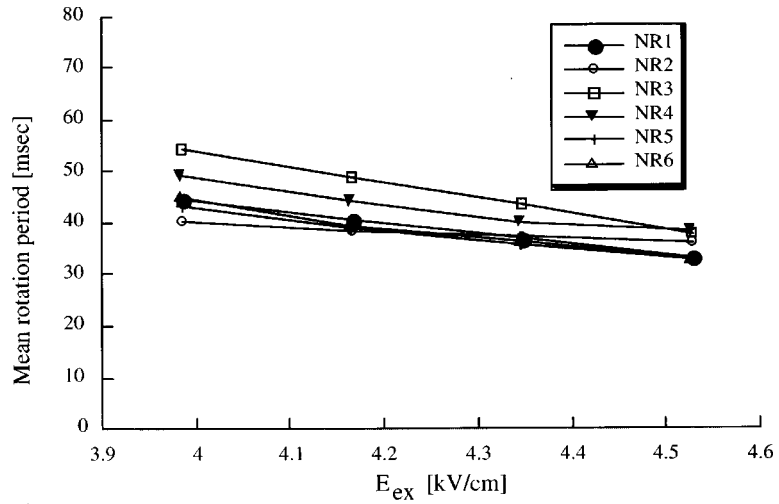


(a)

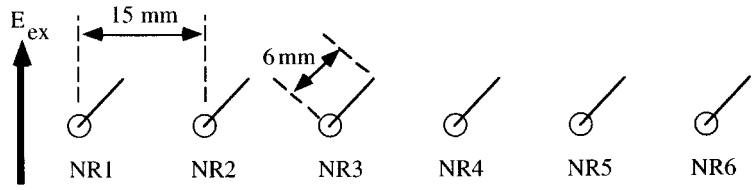


(b)

FIG. 7. (a) Mean rotation period of the individual rotators used in the basic experiment on collective behavior of the needle rotators with the applied external field $E_{\mathrm{ex}}$. (b) Configuration of rotators in $E_{\mathrm{ex}}$. The distance between each neighbor was fixed to 15 mm. Horizontal arm lengths of all rotators were 6 mm.

Each rotator has an individual local coordinate $(r_i,\theta_i,z_i)$ $i=1,2,\ldots,N$, and the position vector of the origin of each coordinate is $\vec{s}_1,\vec{s}_2,\ldots,\vec{s}_N$ in the global coordinate. The horizontal arms of all rotators rotate in the same plane. The values of the field at each rotator are identified by adding the field due to the charge distribution of all the rotators. The electrical field $\vec{E}_i(\vec{l}_i)$ on the rotator $i$ is

$$\vec{E}_i(\vec{l}_i)=\frac{1}{4\pi\epsilon}\int_{A_i+L_i}\frac{\rho_i(\vec{m})}{|\vec{m}-\vec{l}_i|^3}(\vec{m}-\vec{l}_i)dm + \frac{1}{4\pi\epsilon}\sum_{j=1,j\neq i}^{N}\int_{A_j+L_j}\frac{\rho_j(\vec{l}_j)}{|\vec{r}_{ij}|^3}\vec{r}_{ij}dl_j+\vec{E}_{\mathrm{ex}}. \quad (5)$$

The condition that the rotator $i$ is conductor is

$$\vec{E}_i(\vec{l}_i)\cdot\vec{z}_{i0}=0 \quad (\text{on the } A),$$
$$\vec{E}_i(\vec{l}_i)\cdot\vec{r}_{i0}=0 \quad (\text{on the } L). \quad (6)$$

The torque $\vec{T}_i$, that forces on the horizontal arm of rotator $i$, is

$$\vec{T}_i=\int_{L_i}\rho_i(\vec{l}_i)\vec{l}_i\times\vec{E}_i(\vec{l}_i)dl_i. \quad (7)$$

The condition of discharge of the rotator $i$ is assumed as before,

$$\rho_i(\vec{l}_i)>\rho_{i\mathrm{th}}, \quad |\vec{l}_i|=L_i. \quad (8)$$

To carry out numerical simulation the rotator was discretized. The electrical field of any point on the rotator $i$ was expressed as approximated integral equation using discrete charge density $\rho_i(\vec{l}_{ik})$ where $\vec{l}_{ik}$ corresponds to $\vec{l}_i$ in Fig. 9. The part of supporter of rotator $i$ was separated equally to $V$ parts and the part of horizontal arm of one was separated equally to $M-V-1$ parts. That is,

$$\vec{l}_{ik}=\begin{cases}\dfrac{A_i(V-k)}{V}\vec{z}_{i0} & (k=0,1,2,\ldots,V)\\ \dfrac{L_i(k-V)}{M-V-1}\vec{r}_{i0} & (k=V,V+1,\ldots,M-1).\end{cases} \quad (9)$$

$\vec{r}_{ikjl}$ is the vector from $\vec{l}_{jl}$ on the rotator $j$ to the center between $\vec{l}_{ik}$ and $\vec{l}_{ik+1}$ on rotator $i$. The electrical field $\vec{E}_{ik}$ at the discrete position between $\vec{l}_{ik}$ and $\vec{l}_{ik+1}$ on rotator $i$ is

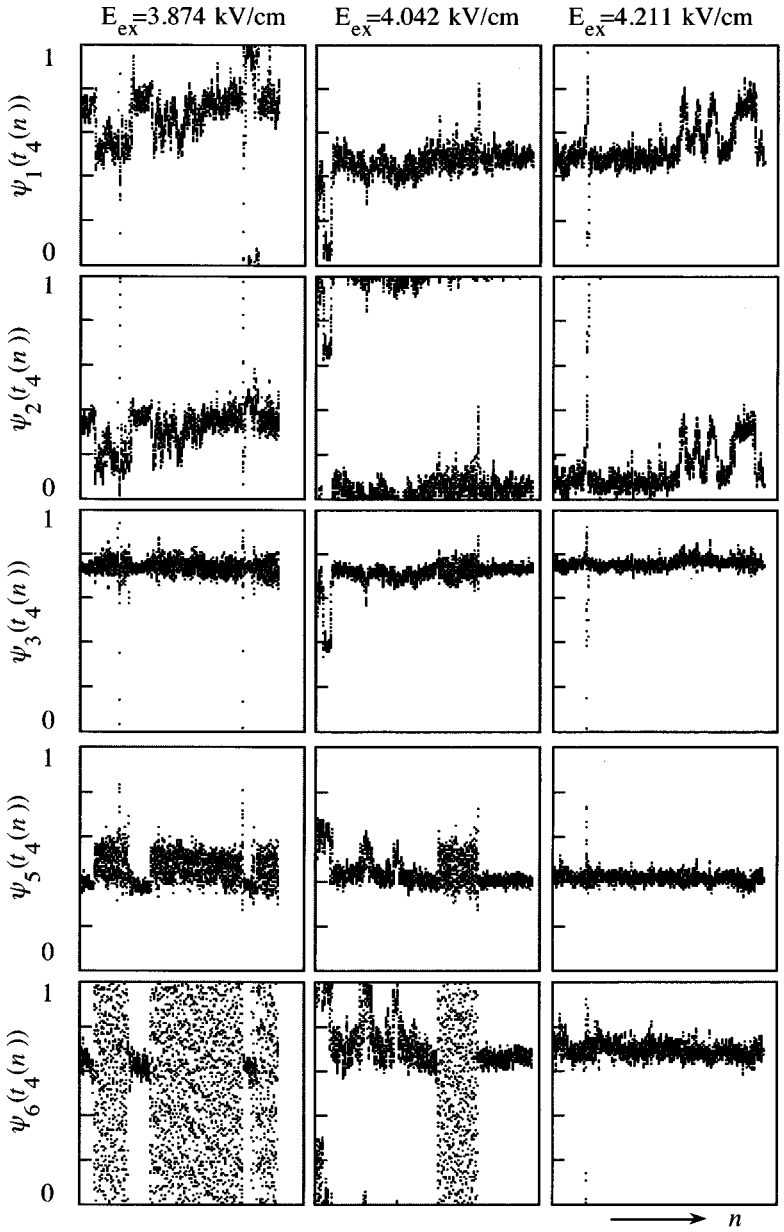


FIG. 8. The sequences of the phase differences measured with respect to that of NR4 in the system with six rotators, NR1, NR2, NR3, NR4, NR5, and NR6 for three different fields.

$$\vec{E}_{ik}=\sum_{j=1}^{N}\frac{h_{jA}}{8\pi\epsilon}\left(\frac{\rho_j(\vec{l}_{j0})}{|\vec{r}_{ikj0}|^3}\vec{r}_{ikj0}+2\sum_{l=1}^{v-1}\frac{\rho_j(\vec{l}_{jl})}{|\vec{r}_{ikjl}|^3}\vec{r}_{ikjl}+\frac{\rho_j(\vec{l}_{jV})}{|\vec{r}_{ikjV}|^3}\vec{r}_{ikjV}\right)+\sum_{j=1}^{N}\frac{h_{jL}}{8\pi\epsilon}\left(\frac{\rho_j(\vec{l}_{jV})}{|\vec{r}_{ikjV}|^3}\vec{r}_{ikjV}+2\sum_{l=V+1}^{M-2}\frac{\rho_j(\vec{l}_{jl})}{|\vec{r}_{ikjl}|^3}\vec{r}_{ikjl}+\frac{\rho_j(\vec{l}_{jM-1})}{|\vec{r}_{ikjM-1}|^3}\vec{r}_{ikjM-1}\right)+\vec{E}_{\rm ex}\quad(k=0,1,\ldots,M-2). \tag{10}$$

Each term in Eq. (10) represents, respectively, the field contribution from each part of the supporters, horizontal arms, and external applied field. The electrical charge $Q_i$ of rotator $i$ is

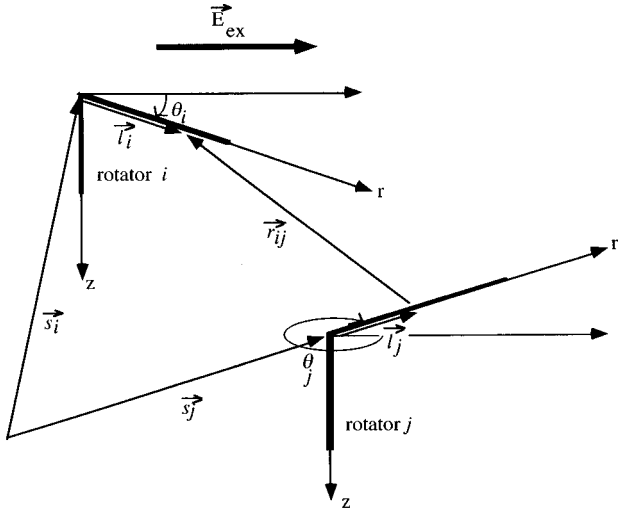


FIG. 9. Definition of the quantities used in the numerical simulation for a pair of rotators. The value of each rotator was identified with subfix $j=1,2,\ldots,N$. $\vec{r}_{ij}=\vec{s}_j+\vec{l}_j-\vec{s}_i-\vec{l}_i$.

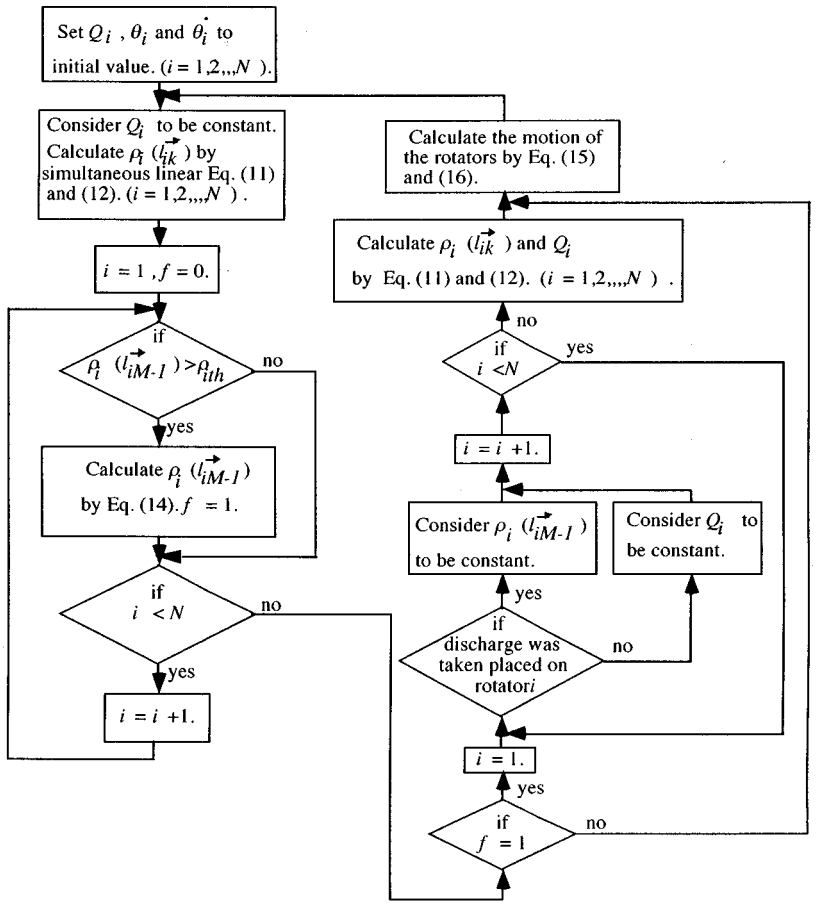


FIG. 10. The flow chart of the numerical simulation.

$$Q_i=\frac{h_{jA}}{2}\left(\rho_i\vec{l}_{i0}+2\sum_{l=1}^{V-1}\rho_i(\vec{l}_{il})+\rho_i(\vec{l}_{iV})\right)+\frac{h_{jL}}{2}\left(\rho_i\vec{l}_{iV}+2\sum_{l=V+1}^{M-2}\rho_i(\vec{l}_{il})+\rho_i(\vec{l}_{iM-1})\right). \quad (11)$$

The condition that rotator $i$ is conductor in the discrete model is

$$\vec{E}_{ik}\cdot\vec{z}_{i0}=0 \quad (k=0,1,2,\ldots,V-1),$$
$$\vec{E}_{ik}\cdot\vec{r}_{i0}=0 \quad (k=V,V+1,V+2,\ldots,M-2). \quad (12)$$

$N\times M$ numbers of $\rho_i(\vec{l}_{ik})$, $i=1,2,\ldots,N$, $k=0,1,\ldots,M-1$ were calculated by simultaneous linear equations (11) and (12). According to Eq. (8) discharge condition was assumed as

$$\rho_i(\vec{l}_{iM-1})>\rho_{ith}. \quad (13)$$

When the condition of Eq. (13) is satisfied, discharge occurs with a time constant $\tau_i$:

$$\rho_i(\vec{l}_{iM-1},t+\Delta t)=(\rho_i(\vec{l}_{iM-1},t)-\rho_{ith})\exp\left(-\frac{\Delta t}{\tau_i}\right)+\rho_{ith}. \quad (14)$$

Equation (14) expresses the charge variation of the rotator $i$ in case of discrete time. If discharge does not occur on any rotators at $t$, $Q_i$ $i=1,2,\ldots,N$ was constant at $t+\Delta t$. So the variables of $\rho_i(\vec{l}_{ik})$ $i=1,2,\ldots,N$ $k=0,1,\ldots,M-1$ were calculated by Eqs. (11) and (12). On the contrary if the discharge occurs on rotator $i$ at $t$, $\rho_i(\vec{l}_{iM-1})$ calculated with Eq. (14) was constant at $t+\Delta t$. Variables $Q_i$, $\rho_i(\vec{l}_{ik})$ $k=0,1,\ldots,M-2$, $\rho_j(\vec{l}_{jm})$ $j=1,2,\ldots,N$ *and* $j\neq i$, $m=0,1,\ldots,M-1$ were calculated by Eqs. (11) and (12). Torque $\vec{T}_i$ was calculated using solved electrical density by Eqs. (11) and (12)

$$\vec{T}_i=h_{iL}\sum_{k=V+1}^{M-2}\vec{l}_{ik}\times\rho_i(\vec{l}_{ik})(\tfrac{1}{2}\vec{E}_{ik-1}+\tfrac{1}{2}\vec{E}_{ik})+\frac{h_{iL}}{2}\vec{l}_{iM-1}\times\rho_i(\vec{l}_{iM-1})(-\tfrac{1}{2}\vec{E}_{iM-3}+\tfrac{3}{2}\vec{E}_{iM-2}). \quad (15)$$

In Eq. (15) it was assumed that the electrical field on rotator $i$ was changed linearly with boundary conditions $\vec{E}_{ik}$, and

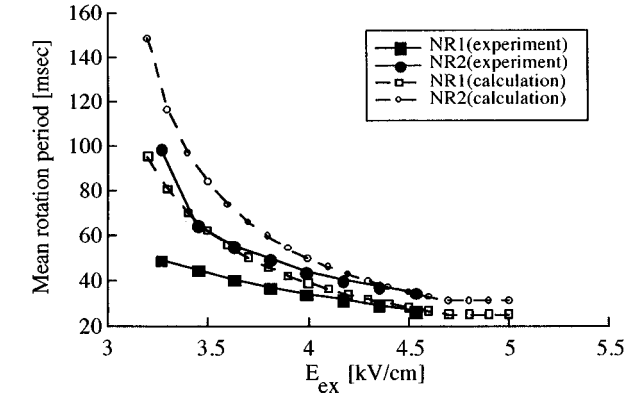


(a)

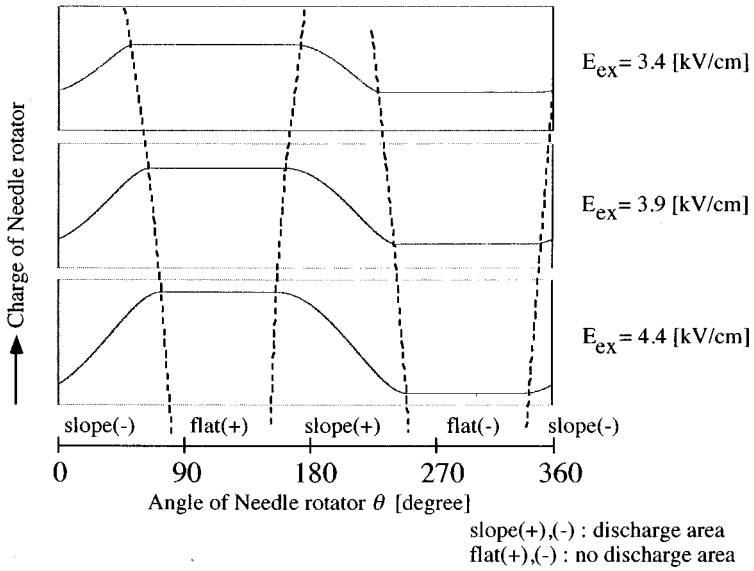


(b)

FIG. 11. (a) Characteristics of the external field $E_{ex}$ vs the mean rotation period of two types of rotators obtained by the experiment and calculation. One of two rotators (NR1) has a horizontal arm length of 8 mm and the other (NR2) has one of 6 mm. (b) Example of the calculated potential of a needle rotator vs its angle for the parameters corresponding to NR2's in Table I. Plots of the cases of three different $E_{ex}$ are shown. The dotted lines are rough border between different states of discharge.

that the field on the edge of rotator $i$ was the field extended from the linear field in the neighbor area. The equation of motion of rotator $i$ is

$$I_i\ddot{\theta}_i+\alpha_i\dot{\theta}_i=T_i\,. \tag{16}$$

$I_i$ is the inertia of rotator $i$, and $\alpha_i$ is its coefficient of damper. The flow chart of the numerical calculation is illustrated in Fig. 10

## V. RESULT OF SIMULATION

### Single rotator

Figure 11(a) shows calculated characteristics of the single rotators together with those of the experiment. The result of calculations shows a reasonable overall agreement, but did not agree with those of experiment in the area of weak field. This discrepancy may be caused by the approximation of the model, as discussed below.

Figure 11(b) shows characteristics of the potential of the needle rotator vs its angle. Two stationary states that occur for different initial conditions are shown in Fig. 12. These results correspond to the results of the experiment, respectively, in Figs. 2(c) and 3. The calculated results of the dynamics of single rotators agree qualitatively with that of experiment.

### Two-rotator system

The mutual dynamics of the rotators were also calculated. The two rotators which were used in this calculation had parameters of NR1 and NR2 shown in Table I. The configuration in applied field was the same as this experiment, as illustrated in Fig. 5(b), except that the distance between rotators was varied in the simulation.

Figure 13(a) shows the result of a calculation of the bifurcation diagram of the time-averaged period ratio with the applied field as the control parameter, for 15 mm of distance between rotators. The initial condition of this calculation was that the angle of the rotator was 0 and the phase velocity was $-200$ rad/s. The calculation started from 3.25 to 4.6 kV/cm of external field, and the method of calculation was similar to that of this experiment. The time step of calculation was $5\times10^{-5}$ s. Calculation data were sampled for $2.9\times10^{5}$

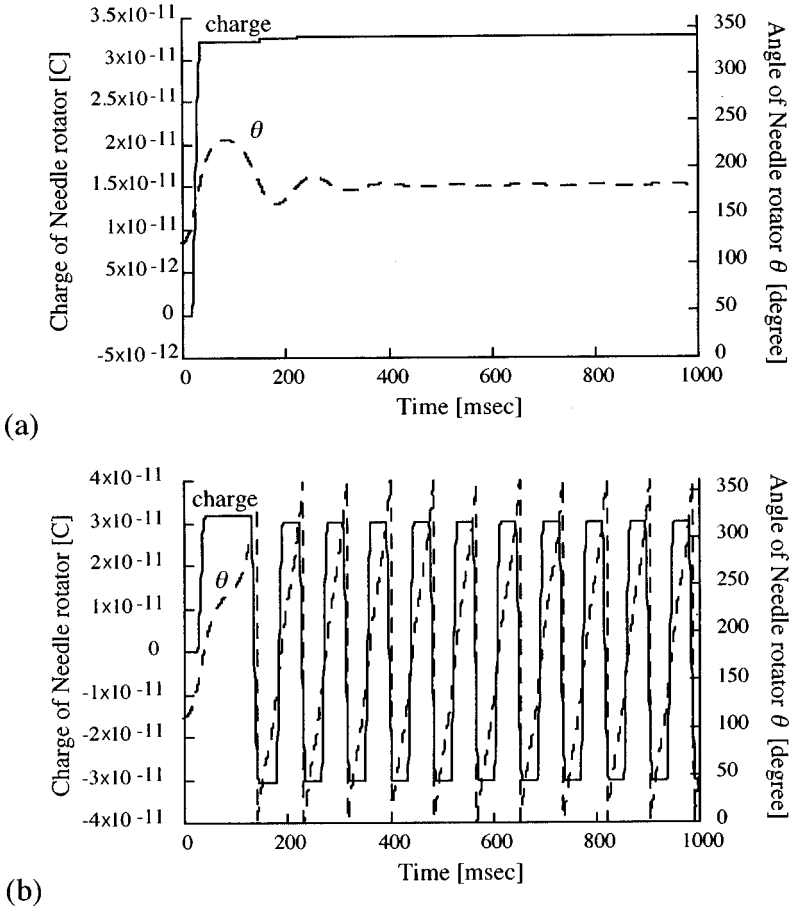


FIG. 12. Two stationary states calculated for different initial conditions for parameters corresponding to NR2's in Table I. The initial condition was given by a step input of an external field of 3.5 kV/cm when the rotator was standing still at a initial angle $\theta_{\text{init}}$ with (a) $\theta_{\text{init}}=120°$ (damping vibration) and (b) $\theta_{\text{init}}=110°$ (nonlinear rotation).

steps after $5\times10^4$ steps from start of each data sampling point. It was confirmed that the dynamics of rotators transited to the steady state after $5\times10^4$ steps which is relatively shorter compared to that of this experiment. Some locking states, which were 3:2, 4:3, and 5:4 of the time-averaged period ratio, were shown in Fig. 13(a). Such locking states were shown in Fig. 6(a) for similar result of the experiment. A hysteresis phenomenon was observed in Fig. 6(a), but not seen in Fig. 13(a).

Figure 13(b) shows the result of the calculation of the bifurcation diagram of the time-averaged period ratio with the applied field as the control parameter, for some distances between rotators. The method of calculation was the same as that of Fig. 13(a), but the simulation were carried out for only one way from 3.25 to 4.6 kV/cm. The time step of the calculation was $1\times10^{-4}$ s. Calculation data were sampled for $3\times10^4$ steps after $2\times10^4$ steps from start of each data sampling point. When the distance between the rotators increases, it is observed that the 3:2 locking state loses its stability more easily compared with other locking states, since the time-averaged period ratios with interaction between rotators take values different from these without the interaction for 3:2 locking state [see Fig. 13(a)].

TABLE I. Parameters setup.

| | NR1 | NR2 |
|---|---|---|
| $L$ (mm) | 8.000 | 6.000 |
| $I$ (kg m) | $2.587\times10^{-11}$ | $1.091\times10^{-11}$ |
| $\alpha$ (kg m $^{-1}$) | $4.100\times10^{-10}$ | $2.085\times10^{-10}$ |
| $\tau$ (s) | $2.222\times10^{-3}$ | $2.222\times10^{-3}$ |
| $\rho_{\text{th}}$ (C) | $4.000\times10^{-8}$ | $2.996\times10^{-8}$ |

The instantaneous relationship between the phase $\psi_2(t_1(n))$ and the ratio of rotating period $T_2(t_1(n))/T_1(t_1(n))$ obtained by numerical simulation shows a good agreement with the experimental observation. Figure 14 shows these relationships for some states shown in Fig. 13(a). There was a permitted range of phase difference for each state as well as the result of the experiment.

### Multi-rotator system

The dynamics of six rotators interacting each other were calculated. All rotators used in this calculation had same parameters of NR1 described in Table I. The relative position of the rotators in the applied field and the names of the rotators are same as the experiment which is illustrated in Fig. 7(b). The time step was $1\times10^{-4}$ s. Sampling data were sampled for $1.2\times10^5$ steps after $4\times10^4$ steps of stabilizing time.

The relationship of the phase difference between the rotators for some initial conditions are shown in Fig. 15. Initial phase velocities of all rotators were $-200$ rad/s. External applied field was 4.5 kV/cm. The initial angles of the rotator patterns were different from each calculation. Figure 15 indicates that this rotator system is a multistable system which has some different steady phase patterns.

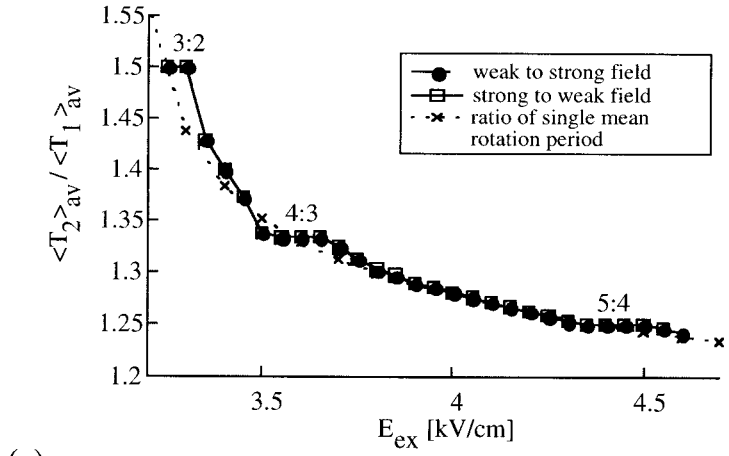


(a)

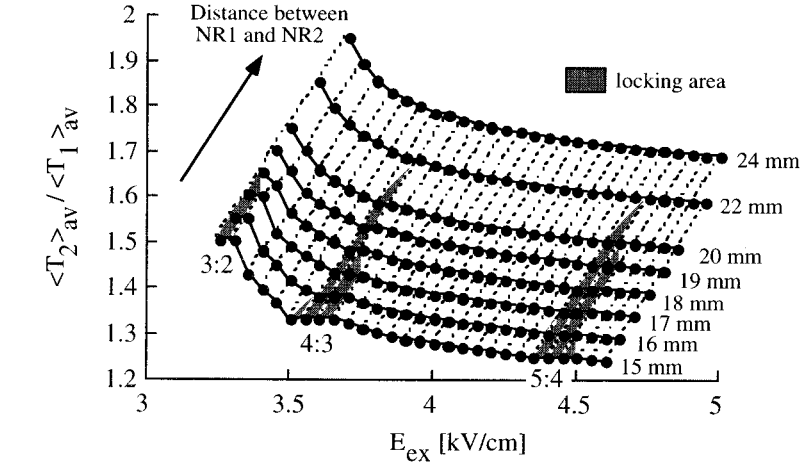


(b)

FIG. 13. (a) Calculated bifurcation diagram of a time-averaged period ratio with the applied field $E_{ex}$ as the control parameter. The time step of the calculation was $5\times10^{-5}$ s. The average was taken for $2.9\times10^{5}$ steps duration starting after $5\times10^{4}$ steps stabilizing time. The broken and solid lines, respectively, show the time-averaged period ratio when the field is increased and decreased. The dotted line shows the calculated ratio of the time-averaged period of noninteracting rotators. (b) Result of the calculation of the bifurcation diagram of the time-averaged period ratio with the applied field $E_{ex}$ as the control parameter for some distance between NR1 and NR2. The time step of the calculation was $1\times10^{-4}$ s. The average was taken for $3\times10^{4}$ steps duration starting after $2\times10^{4}$ steps stabilizing time.

## VI. DISCUSSION

Locking and hysteresis phenomena were observed in the experimental study on mutual dynamics of two different needle rotators. Those phenomena were certainly caused by the mutual effect, as seen in Fig. 6(a). It is necessary to confirm whether the cause of the mutual effect was the Coulomb force between the charge distribution on the needle rotators. One of the other possible causes of coupling is the common fluctuation of the output of the high voltage supply (MAX-ELEC, DPSR-12KPN) by the discharge of the rotators. The influences of the dynamics of the rotator on the output of the supply were shown as voltage fluctuation of the electrodes in Table II. The fluctuation of the rotating state was larger than that of the nonrotating state. The effect of this fluctuation could be ignored because this value was 10 V in the order of magnitude at best.

Another considerable cause is the fluid dynamical effect of charged gas caused by the discharge of the rotators. To investigate the existence of the hydrodynamic effect, we placed a glass plate between rotators NR3 and NR4 used in Fig. 7(a) to examine the effect of the flow of charged gas between the rotators. Figure 16 shows the returned map of the phase difference $\psi_2(t_3(n))$. As seen from Fig. 16, the two rotators were in the 1:1 locking state, which shows the existence of coupling, with the glass plate or not. The deviation of the distribution of those situations in Fig. 16 might probably be caused by the effect of the polarization charge of the glass plate.

Therefore, we can conclude that the observed phenomenon of coupling in this experiment was assumed to be caused by the Coulomb force between the needle rotators. Since the locking phenomena are observed in the case that the distance between two rotators is over 30 mm (not shown here), the interaction of the rotator system is of long range.

The bifurcation which was shown in Fig. 6(a) illustrated a route to chaos through some locking states, which was called ''Arnold's tongue'' [8]. Figure 17 illustrates the returned maps of unlocking states $Y$ and $Z$ in Fig. 6(a). The folding structure was seen in Fig. 17(b), but not seen in Fig. 17(a). This is one of the characteristics of the chaos. Although only one route of Arnold's tongue was shown in this experiment, future detailed investigation may clarify the full structure of Arnold's tongue for the needle rotator system.

A feature of the locking phenomenon was that the phase difference of the two rotators was localized in a region of phase-difference space. As seen in Fig. 6(c), 1:1 locking states become more and more unstable as the phase difference approaches 0. When two rotators are rotated in phase, at $\theta_1=\theta_2=0°$ or 180°, where the torque by the interaction could act most effectively, the torque by the interaction act-

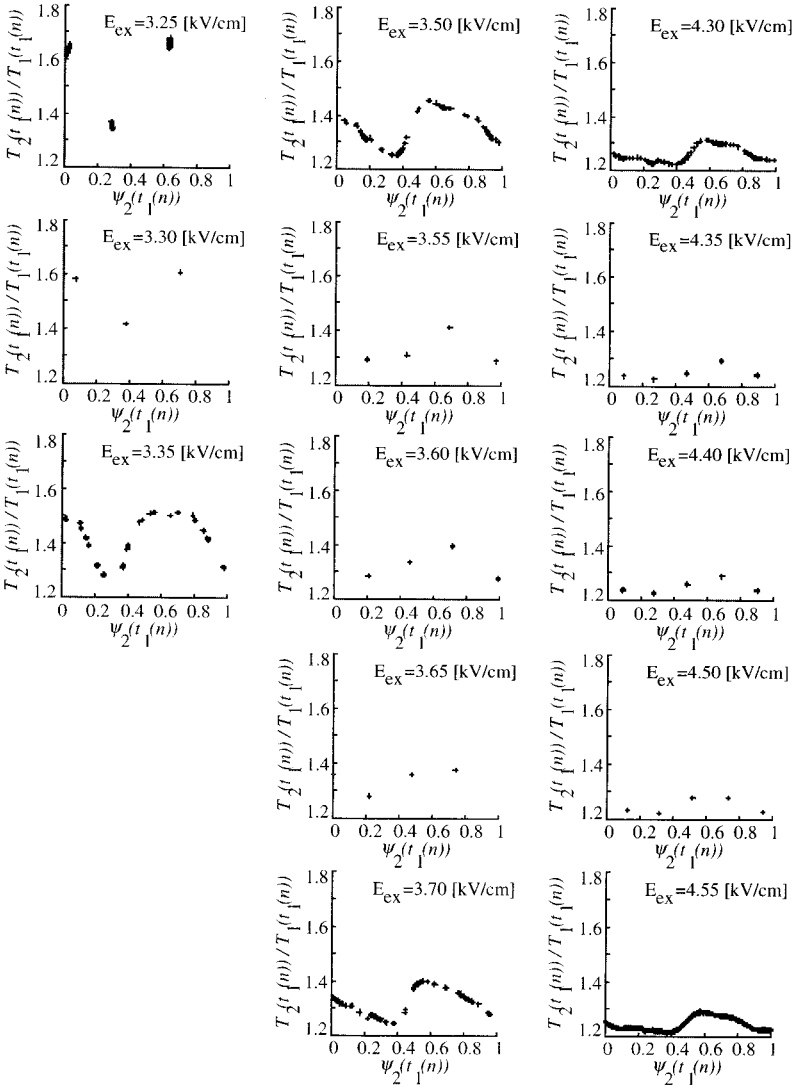


FIG. 14. The distribution of an instantaneous relationship between the phase $\psi_2(t_1(n))$ and the ratio of rotation periods $T_2(t_1(n))/T_1(t_1(n))$ for some plots in Fig. 13(a). The horizontal and vertical axes of each graph correspond, respectively, to $\psi_2(t_1(n))$ and $T_2(t_1(n))/T_1(t_1(n))$. The graphs in the left column, center column, and right column, respectively, correspond to the graphs near 3:2 locking, 4:3 locking, and 5:4 locking.

ing upon a rotator is in a direction opposite to that acting upon another rotator [see Fig. 18(a)]. Since the sense of rotation of the rotators were the same as each other, the rotation in phase was not stable. Conversely, if two rotators rotate in an opposite phase, at $\theta_1=270°$, $\theta_2=90°$ where the torque by the interaction could act most effectively, the torque by the interaction acts upon each rotator in same direction [see Fig. 18(b)]. That is, rotation in an opposite phase should be stabilized.

The reason there is a certain degree of region of phase difference where the mutual dynamics could keep the locking state is due to the inertia of the rotators. That is related to the hysteresis phenomena which were observed in this experiment.

The model of the needle rotator proposed in this paper was a discretized model with the approximation that the rotator could assume an L-shaped line. Although agreement between the results of the calculation for the dynamics of a single rotator and the result of the experiment was qualitatively excellent, it is quantitatively not satisfactory. This means that some part of the model, such as the threshold condition of the discharge, might have to be improved.

The locking phenomena obtained by the simulation shown in Fig. 13 would support a conclusion that the observed locking phenomenon is caused by the Coulomb force in the experiment. Figure 19 is the returned map of $\psi_2(t_1(n))$ of an unlocking state in Fig. 13(a). The negative slope around $\psi_2(t_1(n))=0.4$ in Fig. 19 might suggest the

TABLE II. The voltage dispersion of the electrodes.

| | Standing still state ($\theta=180°$) | | Rotating state | |
|---|---|---|---|---|
| Applied field (kV/cm) | +electrode (kV$^2$) | −electrode (kV$^2$) | +electrode (kV$^2$) | −electrode (kV$^2$) |
| 3.623 | 0.001 378 9 | 0.001 673 4 | 0.001 443 1 | 0.001 761 6 |
| 4.528 | 0.001 840 9 | 0.002 277 9 | 0.001 902 2 | 0.002 645 6 |

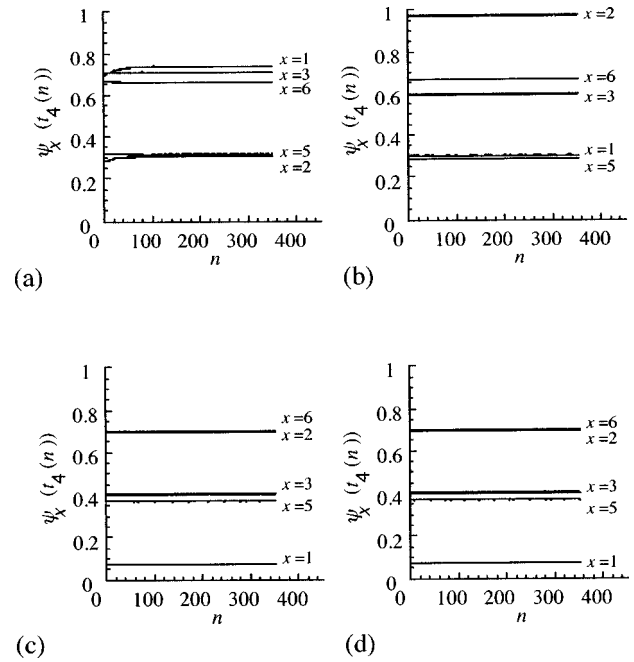


FIG. 15. The calculated sequences after $4\times10^4$ steps from the start of the phase differences with respect to that of NR4 for some initial conditions. Initial phase velocities of all rotators were $-200$ rad/s. The external applied field was 4.5 kV/cm. (a) Initial angle of rotator pattern $(\theta_1,\theta_2,\theta_3,\theta_4,\theta_5,\theta_6)=(0,0,0,0,0,0)$. (b) Initial angle of rotator pattern $(\theta_1,\theta_2,\theta_3,\theta_4,\theta_5,\theta_6)=(0,90,180,270,0,90)$. (c) Initial angle of rotator pattern $(\theta_1,\theta_2,\theta_3,\theta_4,\theta_5,\theta_6)=(0,0,180,180,180,180)$. (d) Initial angle of rotator pattern $(\theta_1,\theta_2,\theta_3,\theta_4,\theta_5,\theta_6)=(0,45,90,135,180,225)$.

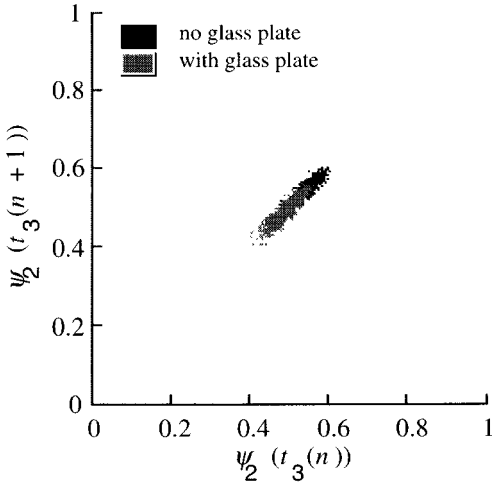


FIG. 16. The returned map of the phase difference $\psi_2(t_3(n))$ with and without a glass plate between the rotators. The phase difference $\psi_2(t_3(n))$ were measured from the mutual dynamics of NR3 and NR4 which were shown in Fig. 6(a). The distance between two rotators was 14 mm. The glass plate ($50\times100$ mm$^2$, 0.5 mm of thickness) were set at the middle point of the two rotators because of the cutting off from the charged gas caused by the discharge of the rotators.

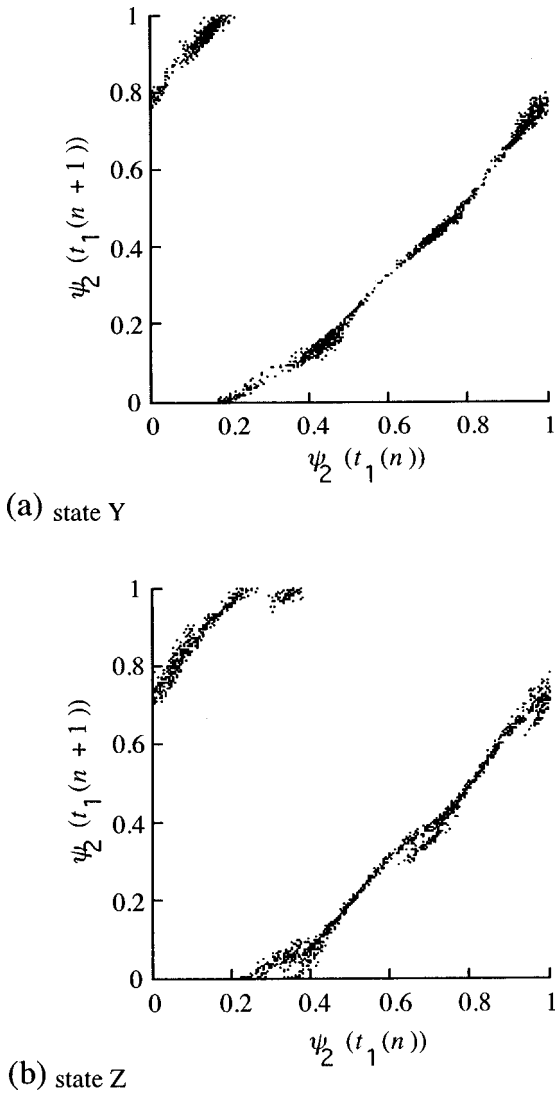


FIG. 17. The returned map of the phase difference $\psi_2(t_1(n))$ for two states in Fig. 5(a). (a) The returned map for state $Y$. (b) The returned map for state $Z$.

existence of chaos around unlocking states, although the existence of chaos was not confirmed in the experiments. No hysteresis phenomenon was obtained in the result of the calculation shown in Fig. 13(a). Comparison of the dynamics for a single rotator between the experiment and the calculation is shown in Figs. 3 and 12. The transition period of the experiment for the change of the field was slower than that of the calculation, which means that it is more difficult to break a locking state between the rotators in the experiment than in the simulation. Since the response time for the variation of the external applied field depends on the inertia of the rotators and the time constant of the discharge, there may still be a possibility to improve the hysteresis phenomenon by better selection of these parameters in the simulation.

In Sec. III, two cluster formation of the 1:1 locking clusters was reported (Fig. 8). One of them was constructed with NR1 and NR2, and another with NR3, NR4, NR5, and NR6. As each pattern was maintained in a certain time, the system of needle rotators was a multistable system.

Cluster formation phenomena were also reported [5] in the study of coupled Ginzburg-Landau (GL) equations with a

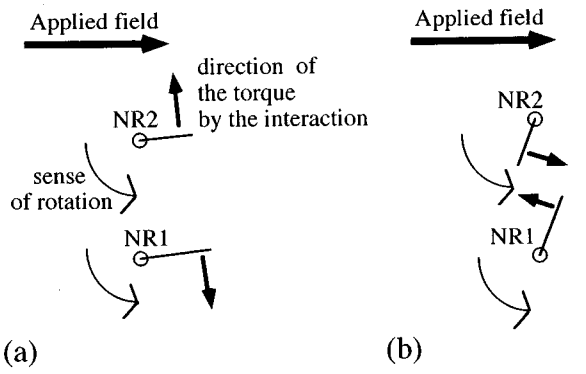


FIG. 18. Figures showing that the state of out of phase rotation has a stronger interaction than the in-phase rotation. (a) The case of in-phase rotation. (b) The case of out-of-phase rotation.

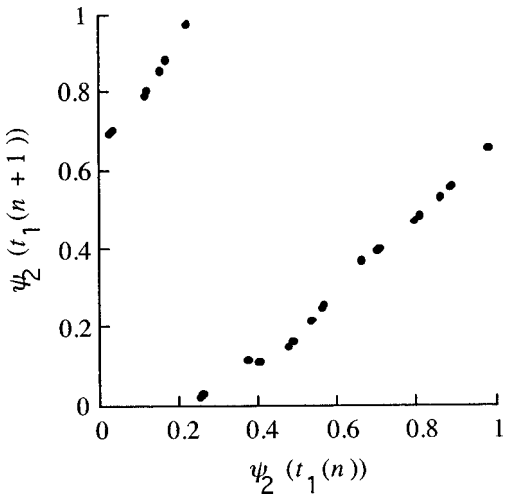


FIG. 19. The returned map of the phase difference $\psi_2(t_1(n))$ for unlocking states in Fig. 13(a). The figure was plotted from the calculated data when the external applied field was 3.35 kV/cm.

medium range of interaction. The apparent similarity of the cluster formation observed in the present experiments and in the coupled GL system may not be fundamental, and the former might be attributed to the inhomogeneity of the experimental system.

The result of the simulation with six rotators showed that there were some 1:1 locking states with different relationships of phases (Fig. 15). Similar phenomena were seen in the result of the experiment (Fig. 8). In the experiment, the existence of some 1:1 states were confirmed as a mixture of different 1:1 locking states. The fluctuation of the phase difference of each rotator of the experiment was larger than those of the calculation shown in Fig. 15. This difference would be caused by the error of the parameters of the rotators, or by some disturbance in the experiment. The transition between different 1:1 locking states would be caused by the fluctuation.

A single rotator might have a similarity to a GL equation, considering the the electrical charge of the rotator corresponds to the amplitude of the GL equation [5]. The mutual interaction between the GL equation is a periodic function of the phase difference of two oscillators, but the interaction of the present model is not only a function of phase differences but also depends on the phases of individual rotators with respect to the position of the electrode. This different nature of the interaction may be responsible for the difference of the behavior between the model and the GL system.

## VII. CONCLUSION

We experimentally investigated nonlinear dynamics of a coupled oscillator system by using charged needle rotators which rotate in a strong electric field and discharge. The result of the experiment for two rotators which had different horizontal arm lengths showed some typical phenomena expected in nonlinear systems, such as the entrainment effect, hysteresis, and chaos phenomena. The mutual dynamics using six rotators which had similar parameters showed 1:1 locking of the mean rotation period of all rotators. Also, the dynamics of six rotators suggested that the needle rotator system could have a multistable system.

The result of the simulation for a needle rotator system indicated a good agreement with that of the experiment. But some improvement of the model may be necessary for a perfect reproduction of the observed phenomenon in detail.

This paper showed that a system consisting of needle rotators could be a real example of a coupled oscillator system with nonlocal interaction. It is possible to study various phenomena in this system, and furthermore the investigation may reveal other unique phenomena of the coupled nonlinear system with a long-range interaction.

[1] Charles M. Gray, Peter Konig, Andreas K. Engel, and Wolf Singer, Nature (London) **338**, 334 (1989).
[2] K. R. Delaney, A. Gelperin, M. S. Fee, J. A. Flores, R. Gervais, D. W. Tank, and D. Kleinfeld, Proc. Natl. Acad. Sci. USA **91**, 669 (1994).
[3] S. Watanabe and S. H. Strogatz, Phys. Rev. Lett. **70**, 2391 (1993).
[4] Jeremy Levy and Mark S. Sherwin, Phys. Rev. Lett. **68**, 2968 (1992).
[5] Y. Kuramoto, Prog. Theor. Phys. **94**, 321 (1995).
[6] N. Nakagawa and Y. Kuramoto, Physica D **75**, 74 (1994).
[7] S. Chiba and Y. Sawada, J. Phys. Soc. Jpn. **65**, 345 (1996).
[8] See, for example, P. Berge, Y. Pomeau, and C. Vidal, *Order within Chaos* (Hermann, Paris, 1984), Chap. 7.